

RESEARCH ARTICLE

Reliable online measurement of population dynamics for filamentous co-cultures

Ana M. Palacio-Barrera^{1,2}  | Ivan Schlembach^{1,2}  | Maurice Finger³  |
Jochen Büchs³  | Miriam A. Rosenbaum^{1,2} 

¹Leibniz Institute for Natural Product Research and Infection Biology, Hans-Knöll-Institute, Jena, Germany

²Faculty of Biological Sciences, Friedrich-Schiller-University Jena, Jena, Germany

³RWTH Aachen University, AVT—Biochemical Engineering, Aachen, Germany

Correspondence

Miriam A. Rosenbaum, Leibniz Institute for Natural Product Research and Infection Biology, Hans-Knöll-Institute, Adolf-Reichwein-Str.23, 07745 Jena, Germany. Email: miriam.rosenbaum@leibniz-hki.de

Funding information

Deutsche Forschungsgemeinschaft, Grant/Award Number: priority program SPP2170, project no. 427899901; German Excellence Strategy of the DFG, Grant/Award Number: EXC 2051, project no. 390713860

Abstract

Understanding population dynamics is a key factor for optimizing co-culture processes to produce valuable compounds. However, the measurement of independent population dynamics is difficult, especially for filamentous organisms and in presence of insoluble substrates like cellulose. We propose a workflow for fluorescence-based online monitoring of individual population dynamics of two filamentous microorganisms. The fluorescent tagged target co-culture is composed of the cellulolytic fungus *Trichoderma reesei* RUT-C30—mCherry and the pigment-producing bacterium *Streptomyces coelicolor* A3(2)—mNeonGreen (mNG) growing on insoluble cellulose as a substrate. To validate the system, the fluorescence-to-biomass and fluorescence-to-scattered-light correlation of the two strains was characterized in depth under various conditions. Thereby, especially for complex filamentous microorganisms, microbial morphologies have to be considered. Another bias can arise from autofluorescence or pigments that can spectrally interfere with the fluorescence measurement. Green autofluorescence of both strains was uncoupled from different green fluorescent protein signals through a spectral unmixing approach, resulting in a specific signal only linked to the abundance of *S. coelicolor* A3(2)—mNG. As proof of principle, the population dynamics of the target co-culture were measured at varying inoculation ratios in presence of insoluble cellulose particles. Thereby, the respective fluorescence signals reliably described the abundance of each partner, according to the variations in the inocula. With this method, conditions can be fine-tuned for optimal growth of both partners along with natural product formation by the bacterium.

Ana M. Palacio-Barrera and Ivan Schlembach contributed equally.

This is an open access article under the terms of the [Creative Commons Attribution-NonCommercial](https://creativecommons.org/licenses/by-nc/4.0/) License, which permits use, distribution and reproduction in any medium, provided the original work is properly cited and is not used for commercial purposes.

© 2022 The Authors. *Microbial Biotechnology* published by Society for Applied Microbiology and John Wiley & Sons Ltd.

INTRODUCTION

Defined co-culture emerges as an interesting new approach for the production of valuable compounds (Minty et al., 2013; Scholz et al., 2018; Shahab et al., 2018; Zhao et al., 2018). Thereby, especially filamentous microorganisms offer great potential, due to their outstanding enzyme production capabilities and metabolic versatility (Mast & Stegmann, 2019; Meyer et al., 2020). The central variable to analyse and optimize co-culture processes is the population composition and its dynamics. Especially when measured online at high temporal resolution, the influence of other process variables can be precisely linked to co-culture behaviour. This gives essential information to find a suitable process window that assures the survival of all different species involved in the system, as well as the biosynthesis of the desired compound. However, monitoring the individual population dynamics of each partner organism and degree of cooperation between them is rather difficult, even more, when cultivated in presence of insoluble particles such as cellulose. Recently, a non-invasive method based on scattered light spectra for determining the population dynamics of defined co-cultures has been reported (Geinitz et al., 2020). However, in contrast to the described research that deals with single-cell microbial systems, filamentous microorganisms have a much more complex and dynamic morphology. Since scattered light is strongly affected by morphology, such method is not applicable to filamentous microorganisms. Furthermore, scattered light cannot readily be applied in presence of insoluble particles such as cellulose.

Alternatively, monitoring of autofluorescence originating from biogenic fluorophores (tryptophan, NADH and flavins) (Pöhlker et al., 2012) has been utilized for the estimation of biomass growth and metabolic activity in axenic cultures (Faassen & Hitzmann, 2015; König et al., 2018; Schlembach et al., 2021; Surribas et al., 2006). However, for co-cultures with similar origin of autofluorescence this approach is difficult to be applied. Furthermore, the autofluorescence signal per cell fluctuates in terms of intensity over time as well as depending on process conditions (Ödman et al., 2009; Schlembach et al., 2021).

For this reason, tagging co-culture partners with different fluorescent proteins becomes a promising, straight-forward alternative to estimate growth and population dynamics. If a constitutive promoter is used to drive cytoplasmic fluorescence protein expression, online fluorescence measurements can be directly correlated with the cell dry weight (CDW) of the corresponding organism. However, this only holds true as long as the cytoplasmic fluorescence protein concentration stays constant. Problems may arise from inhomogeneities of the culture, for example old cells could accumulate more fluorescent proteins than young cells.

Furthermore, even promoters reported to be constitutive, can still show dynamic expression depending on the conditions (Bohle et al., 2007). Therefore, synthetic expression systems, which are independent of the host metabolism are recommended (Rantasalo et al., 2018). Furthermore, weak promoters are recommended to avoid metabolic burden and conserve the wild-type phenotype. Because of these possible biases, it is of utmost importance to validate the robustness of the correlation to biomass formation to ensure that the fluorescence signal is suitable to describe the growth of different organisms in a co-culture.

Besides a proper constitutive expression system, another determining factor for the robustness of the method is the choice of the fluorescence protein. Thereby, the maturation time of the protein is important. If it is too large in comparison to the growth rate of the organism, the fluorescence signal will be dim and lag behind the true biomass growth, corrupting accurate time-resolved measurements (Balleza et al., 2018; Nordholt et al., 2017). The maturation is linked to chromophore formation, which for most fluorescent proteins requires availability of molecular oxygen (Macdonald et al., 2012). This necessity of oxygen for maturation has been reported to be problematic for direct CDW/fluorescence correlations (Drepper et al., 2010). Therefore, oxygen-independent fluorescent proteins have to be chosen under conditions where oxygen limitation is expected to occur. Furthermore, some fluorescent proteins are adversely affected by pH, since the light-absorbing part of the chromophore can become protonated in acidic media (Roberts et al., 2016). For instance, although monomeric GFPs are very popular, their acid sensitivity restricts their application under conditions, where intracellular pH is expected to fluctuate (Cranfill et al., 2016; Shinoda et al., 2018).

Regarding the spectral properties of the proteins, excitation and emission wavelengths should be chosen to avoid spectral overlap, but also considering the analytical capacity of available devices. As rule of thumb, the use of GFP/RFP (green/red) or CFP/OFP (cyan/orange) tags instead of GFP/YFP (green/yellow) or GFP/OFP (green/orange) fluorescent proteins is recommended (Kleeman et al., 2018; Shaner et al., 2005). However, the choice of pair of fluorescent tags could change according to the demands of the bioprocess itself, for example if other fluorescent metabolites are to be measured in addition to population dynamics. Also, autofluorescence can spectrally interfere with the measurement. When measuring target fluorescent proteins in co-cultures of labelled strains, it must be considered that the autofluorescence of both microorganisms can bias the measurements. A solution for this constraint is the application of the spectral unmixing method reported by Lichten et al. for pure cultures of a *Saccharomyces cerevisiae* strain labelled with GFP (Lichten et al., 2014).

This method could also be applied to co-cultures, if confirmed that the metabolite(s) causing the autofluorescence bias in emission is (are) the same for both microorganisms or share the same spectral fingerprint (e.g., tryptophan, NADH or flavins). If this prerequisite is not properly assessed, the unmixing of the raw green fluorescence signal will be inaccurate.

Finally, and of utmost importance for complex filamentous organisms, it should be examined, how the different morphological traits interplay with the fluorescence-to-CDW and fluorescence-to-scattered light correlation. The penetration of excitation and emission light might be considerably different in dispersed cultures compared to pelleted cultures.

In the present work, we applied the proposed fluorescence tagging strategy to monitor population dynamics of a cellulose-degrading model co-culture consisting of the industrially relevant cellulolytic fungus *Trichoderma reesei* RUT-C30 and the non-cellulolytic filamentous bacterium *Streptomyces coelicolor* A3(2), which produces antibiotically active pigments, such as actinorhodin or undecylprodigiosin. We first validated the method by correlating fluorescence signals directly to dry biomass as well as scattered light as alternative biomass indicator. Then the robustness of the correlation was assessed under different conditions, including different micro and macro morphologies. Furthermore, spectral unmixing was established to isolate specific green fluorescent protein signals from non-specific green autofluorescence signals in co-cultures. As proof of principle, the method is applied to measure the population dynamics of the target co-culture of a selected green-tagged *S. coelicolor* with a red-tagged *T. reesei* at different inoculations ratios. With this approach, we present a widely applicable strategy to obtain reliable real-time data for population dynamics in defined co-cultures with special emphasis on the pitfalls concerning filamentous organisms.

RESULTS AND DISCUSSION

Comparison of autofluorescence for individual co-culture partners and selection of appropriate fluorescence protein tags

To aid the choice of suitable fluorescence proteins, the autofluorescence was first profiled by measuring full multiwavelength 2D (excitation/emission) fluorescence scans of the non-tagged partner organisms *S. coelicolor* A3(2) and *T. reesei* RUT-C30 at the end of the cultivation. As shown in Figure 1A,B, the autofluorescence encompasses the spectral range of several blue and green fluorescent proteins, while the red fluorescence area (e.g., mCherry) is free of autofluorescence. Consequently, mCherry with its desirable features such

as low maturation time and low pK_a was chosen for tagging *T. reesei*.

For *S. coelicolor*, green fluorescent proteins were chosen despite overlapping autofluorescence, because it can produce red fluorescent metabolites in the higher wavelength area (Tenconi et al., 2013). These are interesting targets to analyse how population dynamics of co-cultures affect natural product biosynthesis. Hence, we intend to simultaneously measure these metabolites by fluorescence in addition to the population dynamics in future research (Finger et al., 2022). The different candidate proteins EGFP, mNeonGreen and bfoGFPa1 were selected based on desirable traits such as low maturation time and low pK_a (Table S1), as reviewed in the introduction.

Online characterization of tagged partners: Green-tagged *S. coelicolor* strains and *T. reesei* mCherry

Evaluation of different green fluorescent labels for *S. coelicolor* and validation of spectral unmixing

As a next step, the most suitable green FP was chosen among the three candidate proteins; EGFP, mNeonGreen and bfoGFPa1. To avoid expression bias due to metabolic burden, a weak constitutive promoter was chosen to drive protein expression. Candidate strains were compared to the parental strain in terms of growth kinetics, morphology and pigment formation. All strains conserved pellet-forming morphology like the WT (Figure S1) and revealed comparable growth kinetics in scattered light measurements (Figure 2A). Such comparable growth was also observed in other growth conditions (Figure S2A). Thus, the natural wild-type phenotype was conserved in the tagged strains and no metabolic burden effects or other bias of FP expression was observed.

However, due to the weak promoter, the green fluorescence of these strains was just slightly higher than the autofluorescence of the wildtype. Therefore, the fluorescent protein signal had to be unmixed from the autofluorescence. This can be done by linear spectral unmixing once the spectral characteristics of the interfering compound are known (Lichten et al., 2014). However, to use this method in co-cultures, it furthermore must be shown that the interfering compound(s) are identical or have the same spectral behaviour in both co-culture partners. To determine the interfering compound, spectral excitation and emission scans of both microorganisms were extracted from the 2D autofluorescence profiles (Figure 1A,B) at the respective maximum emission and excitation wavelengths, normalized and overlaid for comparison (Figure 1C,D). Since the spectra were well overlapping, a common

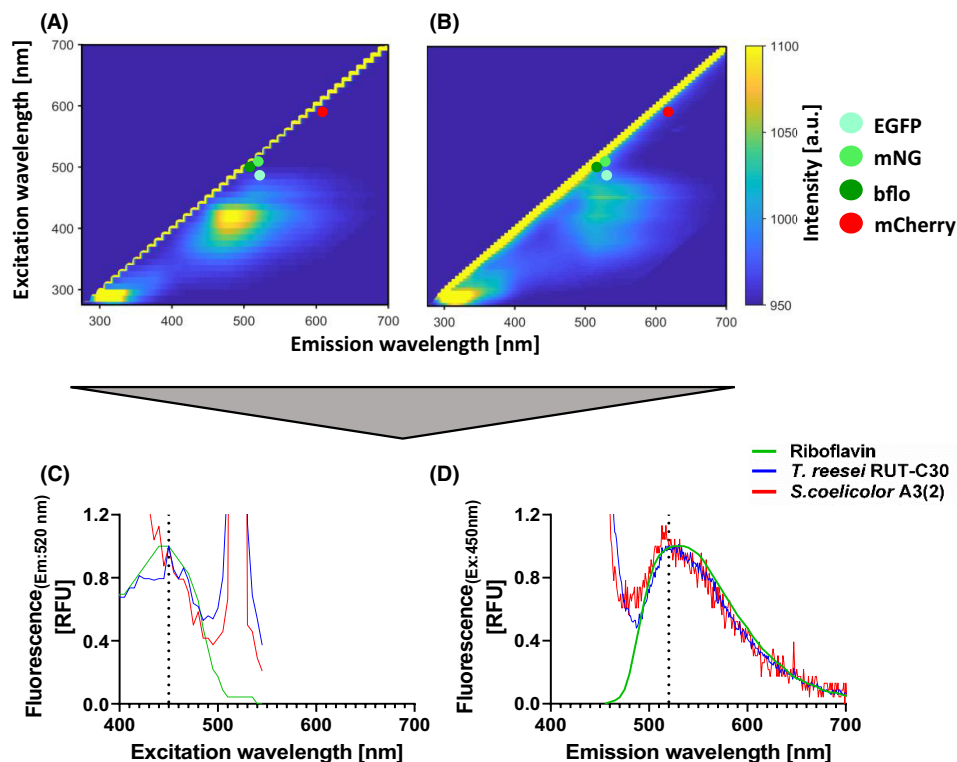


FIGURE 1 Autofluorescence of *S. coelicolor* A3(2) (A) and *T. reesei* RUT-C30 (B). Round symbols indicate the regions of maximum excitation/emission for different fluorescent proteins. Enhanced green fluorescent protein (EGFP), mNeonGreen (mNG), *B. floridae* GFPa1 (bflO) and mCherry. (C) Shows overlay of the excitation spectra of both strains and the biogenic fluorophore riboflavin recorded at 520 nm emission. (D) Shows the overlay of emission spectra of both strains and the biogenic fluorophore riboflavin recorded at 450 nm excitation. The black dotted line marks the maximum of excitation (in C: 450 nm) and the maximum of emission (in D: 520 nm). Strains were grown in axenic conditions in LNP media with 30 g L⁻¹ glucose (100 mM MES) in shake flasks at 30°C and 350 rpm (filling volume: 20 ml, shaking diameter: 50 mm). After 144 h, three wells of a 48-round-well microtiter plate (MTP) were filled with 1 ml of the broth for each culture, and at least three spectra were taken of every well at 30°C and 800 rpm (filling volume: 1 ml, shaking diameter: 3 mm). Samples were scanned in a 2D-BioLector device. Initial spore concentration: 10⁶ spores·ml⁻¹, pH: 6.7 ± 0.2. Depicted data is a representative mean from these measurements.

origin of this green autofluorescence, for example from a common ubiquitous fluorescent metabolite like riboflavin (overlaid in Figure 1C,D) is suggested. This indicates that the method could be used in the targeted co-culture.

To demonstrate the principle of spectral unmixing, WT strain and FP-tagged candidate strains of *S. coelicolor* were grown in a micro cultivation device while online monitoring the fluorescence using two different filter sets (Figure 2B,C). At 480 nm excitation and 520 nm emission, denoted as channel 1, green FP fluorescence was predominantly measured. At 450 nm excitation and 520 nm emission, denoted as channel 2, the autofluorescence was predominantly measured. With these data, a mathematical unmixing of the green FP signal from autofluorescence is possible (Supporting information Method 1, [Lichten et al., 2014]). Comparing the unmixed signals of the green fluorescence protein label in the WT strain and the tagged candidate strains (Figure 2D), it is evident how the signal of the WT strain (which expresses no green FP) is effectively eliminated and stays close to zero. In contrast, the unmixed signals of the tagged strains now describe the expected growth

trend as estimated from the scattered light measurement (Figure 2A,D). This demonstrates the applicability of spectral unmixing in the presented setup. However, when correlating the fluorescence signals to the scattered light (Figure 2E,F), the raw signal of CH1 showed a better correlation to scattered light (Figure 2E) than the unmixed signal (Figure 2F).

This is related to two effects. A phosphate limitation occurs after approx. Seventy-two hour marked by a stress signal in the fluorescence of CH2 (Figure 2C, dotted lines) (Finger et al., 2022), which results in a slowdown of growth. This leads to a plateau in the unmixed signal (Figure 2D), while both raw fluorescence signals continue to increase until or beyond 96 h. This increase in autofluorescence is clearly not related to growth, as the autofluorescence still increases, while the scattered light value levels off. In the correlation plot, this effect leads to a flattening of the correlation. This effect is even more prominent in cultures inoculated with mycelium, which reach phosphate limitation already after 37 h of cultivation (dotted lines across X-axis in Figure S2). Here, it is also evident that the unmixed fluorescence starts to drop simultaneously with

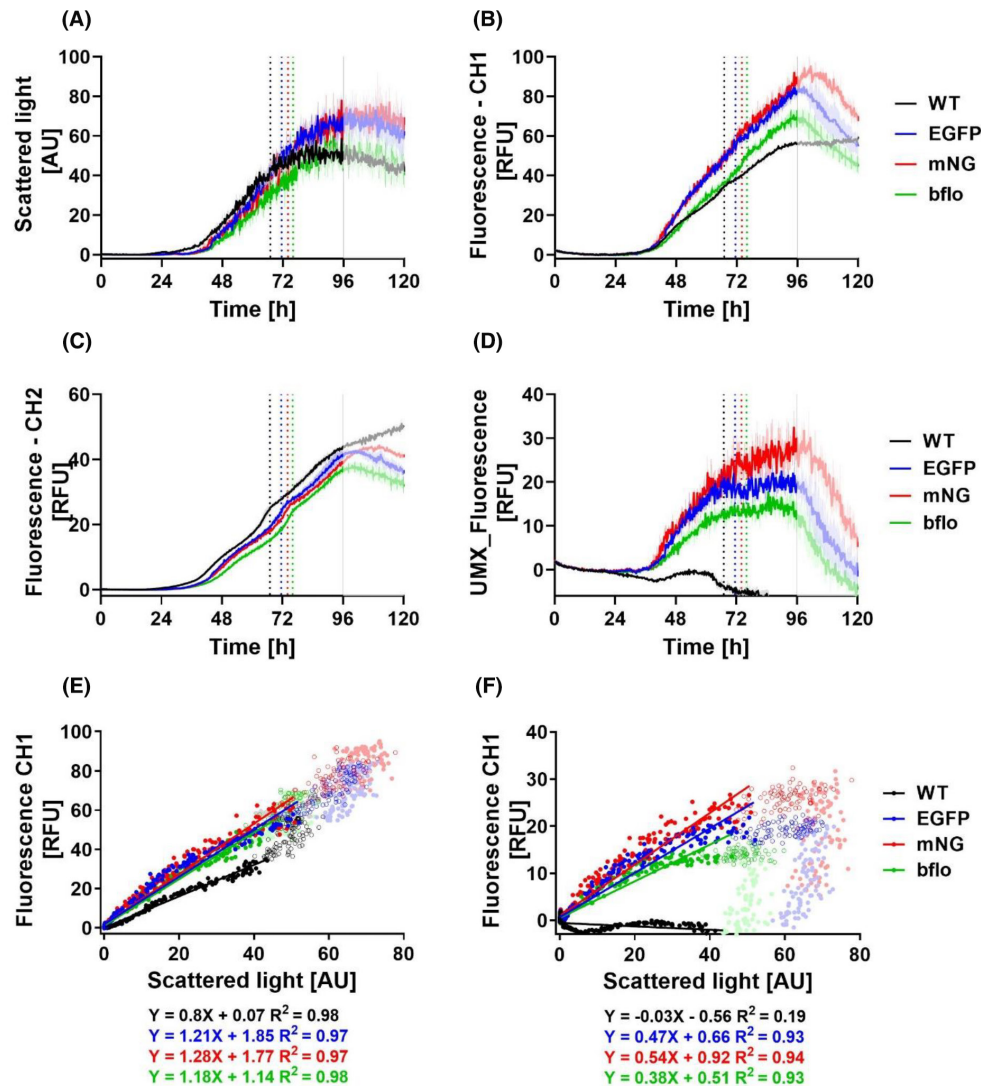


FIGURE 2 Evaluating the use of different green fluorescent proteins for biomass monitoring: Kinetics of scattered light, raw fluorescence, unmixing fluorescence signals and correlation of raw and unmixing green fluorescence to scattered light signal, for spore inoculated cultures of *S. coelicolor* A3(2) WT and derived green-tagged strains. Green tags: Enhanced green fluorescent protein (EGFP), mNeonGreen (mNG), *B. floridae* GFPa1 (bflo). (A) Shows scattered light. (B) Shows fluorescence (as relative fluorescence units: RFU) in channel 1 (CH1—excitation: 480 nm/emission: 520 nm) for a GFP-dominated signal. (C) Shows fluorescence in channel 2 (CH2—excitation: 450 nm/emission: 520 nm) for an autofluorescence-dominated signal. (D) Shows the spectrally unmixed signal extracted from CH1 and CH2 (further details of calculation on materials and methods section and Table S4). (E) Shows correlation of raw green fluorescence plotted to scattered light signal. (F) Shows the correlation of unmixed green fluorescence plotted to scattered light signal. Regression was performed for data from exponential growth phase until phosphate depletion at about 72 h (timing of phosphate limitation is indicated by the coloured dashed lines in A–D). The solid grey line and lighter shaded data points indicate the onset of pigment formation and quenching of the fluorescence signals. In the corresponding parity plots of fluorescence and scattered light (E) and (F), data points acquired after pigment formation were also coloured in lighter shades while data points acquired between phosphate limitation and pigment formation were indicated by hollow circles. This indicates that especially for the unmixed fluorescence (F), the correlation deviates after phosphate depletion and parity not correlating to the biomass anymore after the onset of pigment production. Cultures were grown in LNP media with 30 gL^{-1} glucose (target buffering conditions: 100 mM MES) for 120 h in a 48-round-well optode microtiter plate at 30°C and 800 rpm, initial spore concentration of 10^6 spores ml^{-1} , pH: 6.7 ± 0.2 (filling volume: 1 ml, shaking diameter: 3 mm). Triplicate wells were used for each biological treatment. Solid line in Figure 2A–D corresponds to the mean value, and standard deviation of the growth curves for each biological treatment depicted as a shaded area between error bars. Regression in Figure 2E,F was performed for mean values of the growth curves.

the scattered light signal when entering death phase (marked by arrows in Figure S2), while both raw fluorescence signals continue to increase.

Another important pitfall of the presented method is related to pigment formation. The start of pigment

formation can be determined from a drop in the autofluorescence signal that is owed to quenching effects of the pigment undecylprodigiosin (solid line in Figure 2C), as we demonstrated in a recent publication (Finger et al., 2022). Thereby, the light absorption by the

pigment affects the two fluorescence channels used to unmix the FP signal to different extents (Figure 2B,C). This leads to a corruption of the unmixing calculation and results in a sharp drop of the unmixed signal after 96 h of cultivation (the onset of red pigment formation), which is not seen in the scattered light. Because of this bias, the respective data were disregarded for the calculation of the correlation factor and marked with lighter colour shades (Figure 2F). The data after onset of pigment formation were also marked in Figure 2E, demonstrating that the CH2 signal is more robust against pigment bias. In medium with low buffer concentration and mycelium-inoculated cultures without pigmentation (Figure S2D), this drop in unmixed signal is less pronounced or absent. While this effect might be useful for the optical online estimation of pigment formation, it here prevents accurate biomass and, thus, population dynamics estimation in the targeted mixed culture in late stages after initiation of pigment formation.

Another factor that can bias the fluorescence-to-biomass correlation is pH, which fluctuates throughout the cultivation and might affect the fluorescence depending on the pK_a of the FP. It is not known to what extent the intracellular pH of *S. coelicolor* changes in relation to the extracellular pH. To check for such potential bias, the sensitivity of the specific unmixed fluorescence (Spec UMX_RFU) as indicator of intracellular brightness towards changes in the extracellular pH was evaluated (Figure S3). Thereby, the specific unmixed fluorescence was obtained by dividing the unmixed fluorescence signal by the corresponding value of scattered light. For this purpose, microbioreactor cultures were performed with pH sensing optodes to simultaneously follow the pH online with the fluorescence signals. Because pigmentation interfered with pH measurement, only data before onset of pigmentation were analysed. While it would have been expected that the specific fluorescence would drop clearly for pH values below the respective pK_a of the FP, the specific unmixed fluorescence did not show such trend (see detailed discussion at Figure S3). This indicates that the intracellular pH is relatively robust to changes in the extracellular pH. The latter is consistent with the established capacity of many bacteria for maintaining pH homeostasis (Booth, 1985). Therefore, in our set-up, acid sensitivity of FP-tags is not critical for the targeted conditions. The slight trend of decrease in specific unmixed fluorescence with dropping pH-value (Figure S3A–C) is likely not related to a direct influence of pH on fluorescence of the protein tags. Instead, such decrease is more likely related to the growth dynamics, since the most dynamic change in pH was observed during initial growth phase, which can be deduced from a drop in dissolved oxygen concentration (see detailed example in Figures S3D to S3I).

Finally, since all candidate strains were affected to a similar extent by the described disturbances, the mNeon-Green strain was chosen as target strain for the envisioned

co-culture, because it displayed the highest specific unmixed fluorescence and achieved the best signal-to-noise ratio with the available set-up (Tables S1 and S2). Overall, both raw and unmixed signals in the mNeon-Green strain correlate well to the scattered light and are robust to varying conditions (description in Figure S2), as long as pigment formation is absent. Thereby, the correlation factors tend to have a fluctuation depending on variation in pellet sizes. Finally, the correlation to biomass was independently verified by an additional correlation of the raw signal to offline biomass (dry weight) measurements of *S. coelicolor* grown on glucose (Figure S4). Under non-pigmented conditions, the unmixed signal should be preferred as the raw signal cannot reflect biomass death and further increases while the biomass declines. On the other hand, the raw fluorescence signal is the only possibility to estimate biomass in pigmented cultures. Thus, the most suitable method needs to be selected depending on the respective experimental situation.

Evaluation of the mCherry tag for labelling of *T. reesei* RUT-C30

As for *S. coelicolor*, the *T. reesei* RUT-C30 strain expressing mCherry was also investigated in detail to validate its similarity to the parental strain and to evaluate the robustness of the correlation between fluorescence, scattered light, and biomass under different conditions (Figure 3). As shown in Figure S5, growth behaviour on different carbon sources as well as cellulase production was identical to the parental strain. Furthermore, mCherry fluorescence correlated well with biomass and was robust to changes in cultivation temperature as indicated by the similar slopes of the correlation of 3.0 and 3.8 RFU/g/L at 30°C and 25°C, respectively (Figure S6A). Since the different temperatures led to different growth rates (Figure 3A,B), the correlation is rather growth rate independent. However, under more acidic cultivation conditions using PIPPS buffer, a lower fluorescence per gram of dry biomass was observed, as visible by the lower slope of the regression line of 1.3 RFU/g/L in the PIPPS-buffered cultivation condition (starting pH 5.4), compared to 3.8 RFU/g/L in the more neutral MES buffered cultivation (starting pH 6.7) (Figure S6A). This could be due to a changed, more dense cell composition under these cultivation conditions. Much higher final biomass was reached under the PIPPS condition (15 g L^{-1}) compared with the MES condition (10 g L^{-1}). This is supported by the fact that, in contrast to dry biomass, the fluorescence correlation to the scattered light was excellent in all cases during the early growth phase and followed an identical slope under all tested conditions including the cultivation with PIPPS buffer (Figure S6B). Because the envisioned co-culture will grow on insoluble cellulose particles, the robustness of the mCherry signal as an indicator for

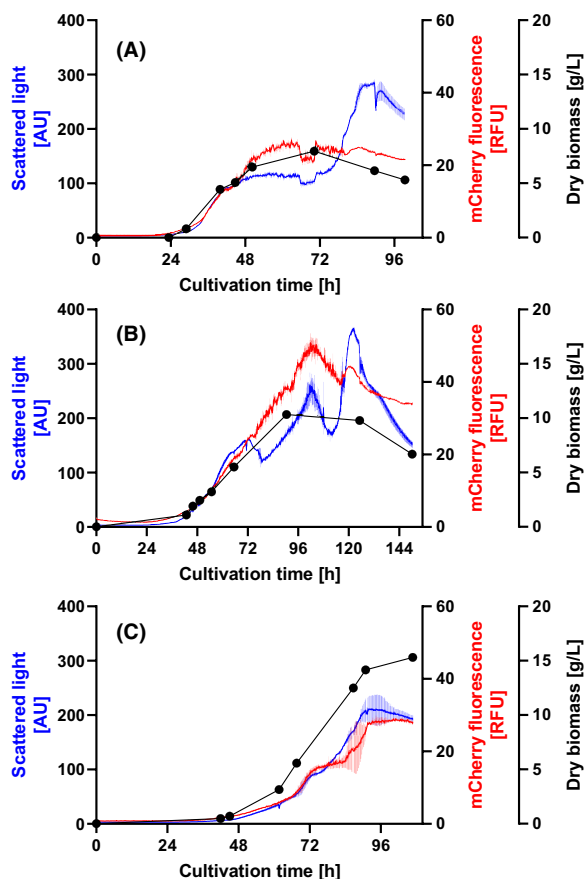


FIGURE 3 Kinetics of mCherry fluorescence, scattered light, and dry biomass during cultivation of *Trichoderma reesei* RUT-C30 mCherry under different conditions. (A) Cultivation in MES-buffered medium (pH 6.7) at 30°C. (B) Cultivation in MES-buffered medium (pH 6.7) at 25°C. (C) Cultivation in PIPPS-buffered medium (pH 5.4) at 25°C. All cultivations were performed with 30 g L⁻¹ glucose as a carbon source in a 48-round-well microtiter at 1200 rpm, 3 mm shaking diameter, 1 ml filling volume and an initial spore concentration of 10⁶ spores ml⁻¹. Data show mean values of independent triplicate wells. The shaded area shows standard deviation. Due to a hardware issue of the Biolector device during the experiment in (C), data from 83 to 91 h were artificially recorded lower than they were. A correction factor was applied for this time frame to align the data to the real curve. For reference, the original data without correction are shown in Figure S13.

fungal biomass was also tested towards varying cellulose concentrations. Therefore, different amounts of biomass were mixed with different cellulose concentrations and the fluorescence signal was analysed. Even in presence of 32 g L⁻¹ of cellulose, the mCherry signal was not affected (Figure S6C).

Effect of biomass morphology on online fluorescence signal for co-culture partners

For a filamentous bacterium like *S. coelicolor* A3(2) varying morphologies can arise during cultivation (i.e.,

clumps or pellets). Thus, it was necessary to evaluate how this affects online measurements of the fluorescence signals. In *S. coelicolor* A3(2), pellet formation varies depending on the culture media and parameters affecting specific power input such as the shaking frequency. From microbioreactors to shake flasks or stirred bioreactors, a heterogeneous pellet size distribution can occur in all cultivations (Zacchetti et al., 2018). We see two main factors besides pigmentation or sporulation that could influence our signals: (1) pellet heterogeneity, which often is a matter of shear forces as well as the presence of spore aggregates in the inoculum, and (2) average pellet size, which is a matter of power input and spore inoculation density.

The effect of heterogeneity was assessed by culturing *S. coelicolor* A3(2)—mNG with solid particles (10 mg glass beads/well) to obtain distinct pelleted forms and the correlation of fluorescence-to-scattered light in the exponential growth phase was assessed. As indicated in Figure 4A, there is no remarkable difference between the slopes of cultures that display a homogenous pellet size distribution and cultures with mixed populations of small and big pellets (Figure 4B, Figure S7A–C). Thus, the correlation of the fluorescence to the scattered light signal is independent of the pellet heterogeneity, when big pellets are present.

However, a clear effect was observed when the average pellet size varied more strongly. To alter the average pellet size, the initial spore concentration for inoculation was changed, which resulted in a more homogeneous distribution of remarkably smaller pellets with the highest spore concentration (Figure 4C,D, Figure S8B). The slope of the correlation of fluorescence to scattered light for the cultures with small pellets increased with decreasing pellets size (Figure 4C). Hence, there was higher fluorescence per scattered light unit. As can be seen from the raw data (Figure S8C,D), this difference was predominantly a result of changes in the scattered light between the different conditions, rather than a change in the fluorescence. Hence, assuming a constant biomass yield, the scattered light signal is more sensitive to changes in morphology than the fluorescence. When analysed by dark field microscopy, the smaller pellets look brighter and seem more transparent, which might indicate that this type of pellets backscatter less light as more light is transmitted.

T. reesei did not show any pellet formation under the tested cultivation conditions. However, other morphologic influences on the optical online signals were observed, depending on the cultivation conditions. Therefore, the fluorescence-to-scattered light correlation was also investigated in more detail for *T. reesei*. As shown in Figure S6B, the correlation was excellent during exponential growth and robust to different cultivation conditions, as mentioned earlier. However, this was not the case for later stages of the cultivation, as can be seen in the extended correlation plots with

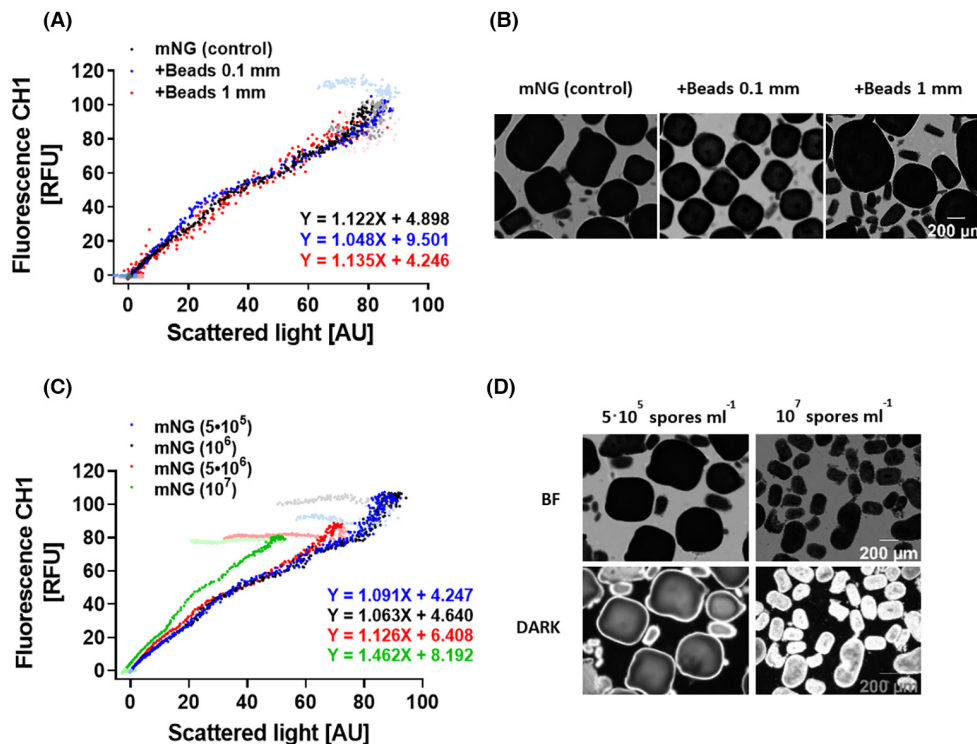


FIGURE 4 Effect of pellet size distributions and homogeneity on the correlation of online green fluorescence signal to scattered light for *S. coelicolor* A3(2) mNeonGreen (mNG). (A) Online fluorescence in channel 1 (CH1—excitation: 480 nm/emission: 520 nm) plotted over the scattered light signal for cultures without (mNG control), and with glass beads (+beads) of 0.1 and 1 mm diameter, respectively. Linear regression was performed only for the growth phase before pigment formation. (B) Bright-field images of cell pellets (5X magnification) displaying varying pellet sizes when cultivated with and without glass beads with an initial spore concentration of 10^6 spores ml⁻¹. (C) Online fluorescence in channel 1 (CH1) plotted over the scattered light signal for cultures without glass beads inoculated with four different spore inoculation densities ranging from 5×10^5 to 10^7 spores ml⁻¹. Linear regression was performed only for the growth phase before drop in scattered light signal due to death phase. Light-coloured points correspond to data after death phase of the culture, which were disregarded for the regression. This is because the raw fluorescence signal cannot indicate a decrease in biomass because it is cumulative and never drops, as discussed earlier. (D) Bright -BF- and dark field -DARK- images of cell pellets (5X magnification) displaying two different major pellet sizes; left column: Lowest spore concentration, right column: Highest concentration. Cultures were grown in LNP media with 30 g L^{-1} glucose (standard buffering: 100 mM MES) for 120 h in a 48-round-well microtiter plate at 30°C and 800 rpm, pH: 6.7 ± 0.2 (filling volume: 1 ml, shaking diameter: 3 mm). Triplicate wells were used for each biological treatment. Regression performed for mean values of the growth curves.

colour-coded morphological changes (Figure S9). At 30°C cultivation, this was because the scattered light signal was strongly increased towards the end of the cultivation due to sporulation of *T. reesei*, while the fluorescence signal indicated the correct biomass trend even after exponential growth (Figure 3A). At 25°C, additionally, a transition from less branched mycelium to a highly branched morphology was observed from 80 to 100 h cultivation (Figures S9 and S10), preceding the sporulation which peaks between 120 h and the end of the cultivation (Figures S9 and S11). This led to a strong increase in scattered light after 72 h cultivation, while the mCherry fluorescence signal and the dry biomass did not show these strong fluctuations (Figure 3B). When sporulation was suppressed by cultivation in more acidic PIPPS-buffered medium (Figure S11), all three signals showed the same trend (Figure 3C). Overall, these results demonstrate that fluorescence seems to be a better indicator for biomass growth than scattered light, because it is much more robust towards morphological changes.

For other research, these differences in sensitivity of fluorescence and scattered light towards morphology might also be useful as an online indicator of morphology to link a characteristic online signal during cultivations with a specific morphological trait. This could be valuable to gain a more detailed understanding of morphology on bioprocesses, similar to recent studies based on imaging flow cytometry for filamentous organisms (Ehgartner et al., 2017; Veiter et al., 2020; Veiter & Herwig, 2019). Such strategies are especially needed for the scale-up of cultures, since morphology is heavily affected by different cultivation settings in stirred tank fermenters.

In summary, the presented results demonstrate that online monitoring of fluorescence is a reliable and robust method for the indirect measurement of biomass for filamentous microorganisms despite some discovered biases. In general, it is to be discussed, what a “reference” way is to describe the abundance of an organism. Many methods are possible, such as number of cell nuclei/ml, projected microscopy area or cell

volume/ml, dry weight/ml, scattered light, turbidity, etc. All these quantifiers have different relations to the microorganism and independently change for each microorganism and cultivation conditions. We, therefore, recommend to regard the online fluorescence signal as cell quantifier by its own and not a replacement, similar to scattered light and dry weight, which all have their own benefits and drawbacks. We tried here to test as many possible biases as possible to investigate the robustness of the method. The result is, that the method does not perfectly correlate with scattered light or biomass in every condition. But it can be also questioned whether the biomass or the scattered light reflects the real abundance of the microorganism. In case of filamentous organisms, we conclude that it could even be better to use fluorescence instead of scattered light-based measurements because the latter is much more prone to bias by morphological variations such as different pellet sizes, different branching patterns or sporulation. In contrast to scattered light, fluorescence can also be reliably applied in presence of turbid media or particulate medium components such as cellulose.

Proof of principle for online monitoring of a filamentous defined co-culture of *T. reesei* mCherry and *S. coelicolor* mNeonGreen

Finally, after validating that phenotypes were identical to the parental strains, and that the correlations between fluorescence and biomass of the two partner organisms are robust under various conditions with varying morphologies, the method was tested in the targeted co-culture setup for estimating the population dynamics.

Co-cultures of *T. reesei* RUT-C30 mCherry and *S. coelicolor* mNeonGreen using different spore inoculation ratios of both partners were grown in a 48-round well microbioreactor using a medium with the insoluble carbon source α -cellulose and a small amount of glucose (5 g L^{-1}) for initial growth. In this setting, *S. coelicolor* relies on secreted cellulolytic enzyme activity of *T. reesei* for growth, after the initial glucose is consumed. As shown in Figure 5, a gradient for each fluorescent signal was obtained, according to the changes in the spore inoculation ratio of each partner. Pigment formation was absent in these co-cultures. Hence, the fluorescence data should be free of pigment bias. The decrease in fluorescence signal for the axenic culture of *S. coelicolor* mNeonGreen (darkest green-black line, Figure 5A), is rather a consequence of biomass death.

The population dynamics of the two organisms are expected to be largely affected by inoculum ratio and the proportion of the respective fluorescence signals correlates well with the inoculum ratios. Thus, it can be concluded that the respective fluorescence tag

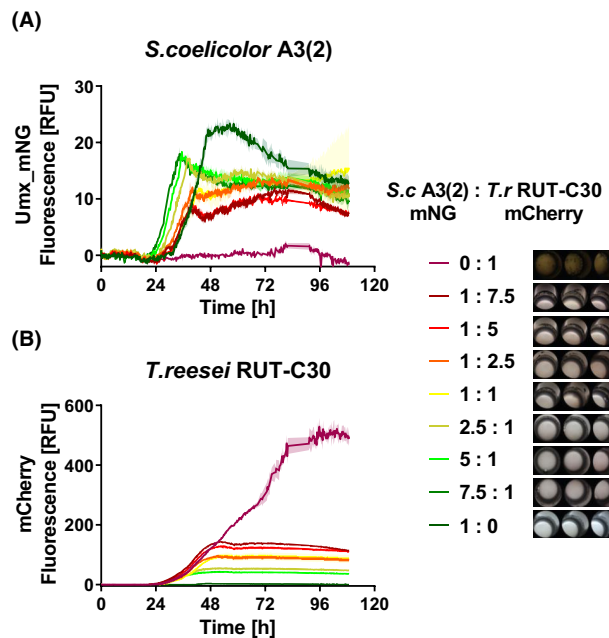


FIGURE 5 Online monitoring of population dynamics for co-cultures of *S. coelicolor* A3(2) mNG and *T. reesei* RUT-C30 mCherry starting with varying spore inoculation ratios. Unmixed mNeonGreen signal (Umx_mNG as relative fluorescence units: RFU) from data obtained of channel 1 (excitation: 480nm/emission: 520nm) and channel 2 (excitation: 450nm/emission: 520nm) showing the growth of *S. coelicolor* A3(2) (A). mCherry signal (as relative fluorescence units: RFU) showing the growth of *T. reesei* RUT-C30 measured at excitation: 580nm/emission: 610nm (B). Well pictures depicted for each inoculation ratio. Dark red line corresponds to highest *T. reesei* mCherry spore concentration, dark green line to highest *S. coelicolor* mNeonGreen. Magenta line corresponds to axenic culture of *T. reesei* mCherry, darkest green-black line to axenic culture of *S. coelicolor* mNeonGreen. Cultures were grown in target culture conditions: LNP media + 5 g L^{-1} glucose and 30 g L^{-1} α -cellulose (standard buffering: 100mM MES), in a 48-round-well microtiter plate at 30°C and 800 rpm. Initial base spore concentration: 10^6 spores ml^{-1} denoted as 1 (filling volume: 1 ml, shaking diameter: 3mm). Triplicate wells were used for each biological treatment. Solid line corresponds to the mean value, and standard deviation of the growth curves for each biological treatment depicted as shaded area between error bars.

effectively described the individual biomass development in the co-culture. Thereby, the data indicate that a high initial inoculum ratio of *S. coelicolor* strongly suppresses the growth of *T. reesei*, while a high initial inoculum ratio of *T. reesei* suppresses growth of *S. coelicolor*, only to much lower extent. This becomes even more obvious, when comparing the respective axenic cultures. This effect could be related to the faster onset of growth of *S. coelicolor*, which outcompetes *T. reesei* for initial glucose and prevents cellulase formation by the latter prohibiting continued growth on cellulose. We can conclude that this co-culture is compatible under the tested growth conditions and each culture sustains growth in correlation to its initial inoculation density, according to the individual fluorescence signals of each partner.

Overall, the results demonstrate the benefits of using fluorescent-tagged organisms to follow population dynamics in a complex system comprising two filamentous microorganisms and an insoluble cellulose substrate. To our knowledge, this is the first demonstration of a method that allows to resolve population dynamics of filamentous organisms in presence of insoluble particles in real-time and non-invasively. Now, this tool for online monitoring of population dynamics in co-cultures opens up new possibilities for further tuning and optimizing of co-cultures for the needs of the bioprocess (i.e., growth rates, enzyme production, secondary metabolite biosynthesis). However, it was also clearly shown that the correlation of online fluorescence to biomass is not valid when pigments are formed that spectrally interfere with the chosen fluorescence tags. Therefore, future work should focus on establishing an optical method for online quantification of the pigment formation, which may allow to quantify the light absorption and fluorescence quenching caused by the pigments, in order to correct the fluorescence signals for these effects.

EXPERIMENTAL PROCEDURES

Microorganisms

The strains *Streptomyces coelicolor* A3(2) DSMZ 40783 and *T. reesei* RUT-C30 were obtained from the Hans-Knöll-Institute—culture collection.

Construction of green tagged *Streptomyces coelicolor* A3(2) strains

For strain construction of *S. coelicolor* A3(2), three green fluorescent proteins with different features as shown in Table S1 were selected. For construction of the *S. coelicolor* A3(2)-*egfp* strain; the *egfp* gene (derived from mutations of *avgfp* -*Aequorea victoria* GFP) encoding for Enhanced Green Fluorescence Protein (EGFP) was obtained from the plasmid pIJ8641 (Table S3) previously constructed for *Streptomyces* strains (Sun et al., 1999). For construction of the remaining strains, the DNA sequences for the *mNeonGreen* (from *Branchiostoma lanceolatum*) and *bflogfpa1* (from *Branchiostoma floridae*) genes were obtained from GenBank (accession: KC295282.1) and the European nucleotide archive (EEN59121.1), respectively. These were codon optimized for *S. coelicolor* A3(2) with the OPTIMIZER online tool (<http://genomes.urv.es/OPTIMIZER/>) and DNA sequences were sent to Eurofins Genomics for synthesis. All genes were inserted into the pNG4 plasmid by restriction cloning, in which gene expression is under control of the constitutive *PerME* promoter; with this plasmid the expression cassettes were integrated into a locus that is known to not

affect the wild-type phenotype—(neutral) (Gonzalez-Quiñonez et al., 2016). Conjugation for transformation of *S. coelicolor* A3(2) was done with a protocol previously described (Kieser et al., 2000). All constructed strains, along with *E. coli* strains and plasmids used for cloning and transformation are depicted in Table S3.

Construction of *T. reesei* RUT-C30 mCherry strain

T. reesei RUT-C30 was transformed with an universal synthetic expression system, the SES_A system, (Rantasalo et al., 2018), to drive stable constitutive mCherry expression independent of other regulating mechanisms. The plasmid B7061 (a kind gift from Dominik Mojzita [VTT Technical Research Centre of Finland Ltd]) consists of a mCherry expression cassette with a promoter consisting of eight binding sites for the synthetic transcription factor Bm3R1-NLS-VP16 and the TEF1 terminator from *T. reesei*. It also contains the expression cassette for expression of the synthetic transcription factor itself as well as a hygromycin resistance cassette, flanked by two *pep4* homology arms for homologous recombination. Plasmid B7061 was transformed into *T. reesei* RUT-C30 genome by the PEG/CaCl₂ protoplast transformation method published by Penttilä et al., using hygromycin as selection marker (Penttilä et al., 1987). Candidate clone colonies were picked and screened for red fluorescence using a green LED (530nm) flashlight and red filter goggles. Fluorescent candidates were then transferred and streaked out multiple times on media containing hygromycin to get stable single spore-derived transformants. Transformant clones were sorted according to their fluorescence intensity and individually assessed for similarity to the parental strain. All work in this study was performed with clone number A3, which showed intermediate fluorescence intensity among the tested clones.

Culture media

Cultivations were performed in LNP media, which is a varied composition of the media reported by Antonov et al. (2017) (Antonov et al., 2017). The medium consists of (NH₄)₂SO₄ 3 gL⁻¹, urea 0.3 gL⁻¹, KH₂PO₄ 0.4 gL⁻¹, MgSO₄·7H₂O 0.5 gL⁻¹, CaCl₂·2H₂O 0.23 gL⁻¹, NaCl 0.05 gL⁻¹, MES buffer 0.1 M, Tween 80 0.01% (v/v), trace element solution 2.5 mL⁻¹. The pH was set to 6.7 and adjusted with 2 or 5 M NaOH, when needed. The composition of the trace element solution is the following: Citric acid 180 gL⁻¹, ZnSO₄·7H₂O 16 gL⁻¹, CoCl₂·6H₂O 2.71 gL⁻¹, Fe₂(SO₄)₃ 2.29 gL⁻¹, CuSO₄ 2.05 gL⁻¹, MnSO₄·7H₂O 1.6 gL⁻¹, H₃BO₃ 0.8 gL⁻¹. For axenic cultures, media without the addition of cellulose was used. A glucose concentration of 30 gL⁻¹ was employed for growth of the two microbial partners to

be analysed by means of multi-wavelength-2D fluorescence scans and for experiments for evaluating the performance of tagged *S. coelicolor* A3(2) strains. Finally, the spectral unmixing in a co-culture was undertaken, considering target conditions of cellulose degradation. Therefore, 30 g L⁻¹ cellulose was added to the base LNP media and only 5 g L⁻¹ glucose was used to boost onset of growth for the strains.

Culture conditions

For all growth experiments, except the 2D scans, which were performed in shake flasks, microbioreactor cultures were undertaken in a BioLector® I device (Beckman Coulter). Forty-eight round-well microtiter plates (MTP-R48-B), or 48 round-well microtiter optode plates (MTP-R48-BOH) were used when required. The initial inoculum density for microbioreactor cultures was 10⁶ spores ml⁻¹, except for the evaluation of pellet size/compactness. For dispersed mycelia pre-inoculum, an initial raw scattered light value of 16 A.U. (OD measured of 0.2) was employed. Cultivation conditions were: 800 rpm (3 mm shaking diameter) and 30°C for up to 120 h (except for cultures intended for spectral analysis). Filter modules of the device for online measurement are shown in Table S2. Triplicate wells were analysed for each biological treatment. The mean value of growth curve data and standard deviation were obtained with the help of the GraphPad software (version 9.3.1).

Spectral analysis of axenic and co-cultures

To determine in which excitation and emission regions autofluorescence takes place for each one of the co-culture partners, strains were grown in axenic conditions in LNP media with 30 g L⁻¹ glucose (100 mM MES) in shake flasks at 30°C and 350 rpm (filling volume: 20 ml, shaking diameter: 50 mm). An initial pH of 6.7 ± 0.2 and spore concentration of 10⁶ spores·ml⁻¹ were used. After 144 h, samples of culture broth were analysed in a 48-round-well microtiter plate (MTP) through multi-wavelength-2D fluorescence spectroscopy (30°C, 800 rpm, filling volume: 1 ml, shaking diameter: 3 mm) in a customized BioLector connected to a fluorescence spectrometer via fibre optics (Ladner et al., 2016). Triplicate shake flasks cultures were used. Three wells were measured as technical replicates for each culture, and at least three spectra were taken of every well.

Proof of principle of spectral unmixing

The method of Lichten et al., 2014 was applied for spectral unmixing after adopting the excitation/emission

parameters for our setups: excitation—480 nm and emission—520 nm, named as channel 1, for measurement of an optical signal characteristic of a EGFP protein tag, and excitation—450 nm, emission—520 nm, named as channel 2, for measurement of an optical signal due to autofluorescence. To unmix the autofluorescence in a co-culture, it must be validated that the autofluorescence in both partners has the same spectral characteristics and that the ratio of emission from channel 2 to that of channel 1 for parental strains (termed here as r_a) is identical for the individual partners and consistent with the value corresponding to the interfering compound. To test this, axenic, non-modified cultures were grown under target conditions (LNP media +5 g L⁻¹ glucose and 30 g L⁻¹ α-cellulose) (Figure S12). Further details of calculation are given in Supporting information Method 1. Triplicate wells were done for each axenic culture. Regression plots in Figure S12 were obtained with the help of the GraphPad software (version 9.3.1).

Online characterization of tagged partners

Green-tagged *S. coelicolor* strains

To determine kinetics of the scattered light, green fluorescence online signals, and specific fluorescence, *S. coelicolor* A3(2) strains were cultured in parallel employing two buffering conditions: 100 mM MES, corresponding to the target conditions in co-culture, and weakly buffered conditions of 50 mM MES. For the latter, two types of inocula were assessed: Spores and precultures from dispersed mycelia. LNP medium was used in all cases and 48-well optode plates were used for online pH measurement. Regressions for correlation factors were obtained with the GraphPad software (version 9.3.1) and performed for mean values of the growth curves. For offline data, at least two samples, each consisting of three separate wells from a 48-microtiter plate were taken and measured in each time point. For dispersed mycelia precultures, strains were grown in 50 ml straight rim flasks with 5 ml LNP media with an initial inoculum density of 10⁶ spores ml⁻¹, fed with 1 ml fresh media at 48 h and left in incubation at 28°C, 130 rpm and a shaking diameter of 50 mm until 60–70 h. Here, 15 stainless steel beads (2–2.5 mm diameter) were added to the cultures as previously reported to disperse the biomass (Borodina et al., 2008).

Evaluation of *T. reesei* RUT-C30 mCherry

T. reesei was cultivated in a BioLector at 1200 rpm, 3 mm shaking diameter, and the indicated cultivation temperature. Cultivations were performed in modified Pakula medium containing (NH₄)₂SO₄ 7.6 g L⁻¹, KH₂PO₄

0.8 g L⁻¹, MgSO₄·7H₂O 0.5 g L⁻¹, CaCl₂·2H₂O 0.23 g L⁻¹, NaCl 0.05 g L⁻¹, Tween 80 0.02% (v/v), trace element solution 2.5 mL⁻¹. Different carbon sources were used as indicated in the respective figure caption. The medium was either buffered with 100 mM MES pH 6.7 or with 100 mM PIPPS pH 5.4. For the initial inoculum, 10⁶ spores ml⁻¹ were used. For offline data, at least three samples were taken and measured.

Effect of morphology on online fluorescence signal for a green-tagged *S. coelicolor* A3(2) strain

S. coelicolor A3(2)—mNG cultures were grown in 48 round-well microbioreactors (MTP-R48-B), without and with glass beads (10 mg/well) of 0.1- and 1-mm diameter. Likewise, to determine the effect of low size pellets, microbioreactor cultures were performed, inoculating these with four different spore concentrations ranging from 5·10⁵ spores ml⁻¹ to 10⁷ spores ml⁻¹. Microscopic images of cell pellets were obtained with a ZEISS Axio Imager.M2 microscope at a magnification of 5X in bright field with a LED intensity of 13% and in dark field with a LED intensity of 30.7% employing an exposure time 30 ms for both. For cultures grown without and with particles, image analysis was performed for a representative image of each biological treatment. For cultures inoculated with increasing spore concentrations, image analysis was performed using four different images for each one of the biological treatments.

Proof of principle for online monitoring of a filamentous defined co-culture of *T. reesei* mCherry and *S. coelicolor* mNeonGreen

Microbioreactor (MTP-R48-B) co-cultures were performed at target culture conditions (LNP media +5 g L⁻¹ glucose and 30 g L⁻¹ α-cellulose) using a spore concentration with an initial base of 10⁶ spores ml⁻¹. From this value, the spore inoculation ratios were varied between 1:7.5 (meaning 10⁶ spores ml⁻¹ of *S. coelicolor* + 7.5 × 10⁶ spores ml⁻¹ of *T. reesei*) to 7.5:1 (meaning 7.5 × 10⁶ spores ml⁻¹ of *S. coelicolor* + 10⁶ spores ml⁻¹ of *T. reesei*), and the culture was online monitored as described above.

ACKNOWLEDGEMENTS

We thank Nils Schuhman for experimental support in the characterization of *T. reesei* RUT-C30 mCherry. Open Access funding enabled and organized by Projekt DEAL. WOA Institution: LEIBNIZ-INSTITUT FÜR NATURSTOFF-FORSCHUNG UND INFEKTIONS BIOLOGIE EV HANS-KNOLL-INSTITUT Consortia Name : Projekt DEAL.

FUNDING INFORMATION

This work was supported by the Deutsche Forschungsgemeinschaft (priority program SPP2170, project no. 427899901) and M.A.R. was supported by the the German Excellence Strategy of the DFG (EXC 2051, project no. 390713860).

CONFLICT OF INTEREST

The authors declare no conflict of interest.

DATA AVAILABILITY STATEMENT

The datasets supporting the conclusions of this study are included within the article and its additional file and are available from the corresponding author upon reasonable request.

ORCID

Ana M. Palacio-Barrera  <https://orcid.org/0000-0002-2910-719X>

Ivan Schlembach  <https://orcid.org/0000-0003-1827-7887>

Maurice Finger  <https://orcid.org/0000-0001-7384-8625>

Jochen Büchs  <https://orcid.org/0000-0002-2012-3476>

Miriam A. Rosenbaum  <https://orcid.org/0000-0002-4566-8624>

REFERENCES

- Antonov, E., Schlembach, I., Regestein, L., Rosenbaum, M.A. & Büchs, J. (2017) Process relevant screening of cellulolytic organisms for consolidated bioprocessing. *Biotechnology for Biofuels*, 10, 1–14.
- Balleza, E., Kim, J.M. & Cluzel, P. (2018) Systematic characterization of maturation time of fluorescent proteins in living cells. *Nature Methods*, 15, 47–51.
- Bohle, K., Jungebloud, A., Göcke, Y., Dalpiaz, A., Cordes, C., Horn, H. et al. (2007) Selection of reference genes for normalisation of specific gene quantification data of aspergillus Niger. *Journal of Biotechnology*, 132, 353–358.
- Booth, I.R. (1985) Regulation of cytoplasmic pH in bacteria. *Microbiological Reviews*, 49, 359–378.
- Borodina, I., Siebring, J., Zhang, J., Smith, C.P., Van Keulen, G., Dijkhuizen, L. et al. (2008) Antibiotic overproduction in *Streptomyces coelicolor* A3(2) mediated by phosphofructokinase deletion. *The Journal of Biological Chemistry*, 283, 25186–25199.
- Cranfill, P.J., Sell, B.R., Baird, M.A., Allen, J.R., Lavagnino, Z., De Gruiter, H.M. et al. (2016) Quantitative assessment of fluorescent proteins. *Nature Methods*, 13, 557–562.
- Drepper, T., Huber, R., Heck, A., Circolone, F., Hillmer, A.K., Büchs, J. et al. (2010) Flavin mononucleotide-based fluorescent reporter proteins outperform green fluorescent protein-like proteins as quantitative in vivo real-time reporters. *Applied and Environmental Microbiology*, 76, 5990–5994.
- Ehgartner, D., Herwig, C. & Fricke, J. (2017) Morphological analysis of the filamentous fungus penicillium chrysogenum using flow cytometry—the fast alternative to microscopic image analysis. *Applied Microbiology and Biotechnology*, 101, 7675–7688.
- Faassen, S.M. & Hitzmann, B. (2015) Fluorescence spectroscopy and chemometric modeling for bioprocess monitoring. *Sensors (Switzerland)*, 15, 10271–10291.

- Finger, M., Sentek, F., Hartmann, L., Palacio-Barrera, A.M., Schlembach, I., Rosenbaum, M.A. et al. (2022) Insights into *Streptomyces coelicolor* A3(2) growth and pigment formation with high-throughput online monitoring. *Engineering in Life Sciences*, 1–10. Available from: <https://doi.org/10.1002/elsc.202100151>
- Geinitz, B., Rehmann, L., Büchs, J. & Regestein, L. (2020) Noninvasive tool for optical online monitoring of individual biomass concentrations in a defined coculture. *Biotechnology and Bioengineering*, 117, 999–1011.
- Gonzalez-Quinonez, N., López-García, M.T., Yagüe, P., Rioseras, B., Pisciotta, A., Alduina, R. et al. (2016) New Φ BT1 site-specific integrative vectors with neutral phenotype in *Streptomyces*. *Applied Microbiology and Biotechnology*, 100, 2797–2808.
- Kieser, T., Bibb, M., Buttner, M., Chater, K. & Hopwood, D. (2000) Growth and preservation of *Streptomyces*. In: *Practical Streptomyces genetics*. Norwich, UK: The John Innes Foundation, pp. 43–61.
- Kleman, B., Olsson, A., Newkold, T., Kofron, M., DeLay, M., Hildeman, D. et al. (2018) A guide to choosing fluorescent protein combinations for flow cytometric analysis based on spectral overlap. *Cytometry Part A*, 93, 556–562.
- König, J.C., Steinwedel, T., Solle, D., Lindner, P., De Vries, I., Hentrop, T. et al. (2018) Development and characterisation of a new fluorescence sensor for online monitoring of bioprocesses. *Journal of Sensors and Sensor Systems*, 7, 461–467.
- Ladner, T., Beckers, M., Hitzmann, B. & Büchs, J. (2016) Parallel online multi-wavelength (2D) fluorescence spectroscopy in each well of a continuously shaken microtiter plate. *Biotechnology Journal*, 11, 1605–1616.
- Lichten, C.A., White, R., Clark, I.B.N. & Swain, P.S. (2014) Unmixing of fluorescence spectra to resolve quantitative time-series measurements of gene expression in plate readers. *BMC Biotechnology*, 14, 1–11.
- Macdonald, P.J., Chen, Y. & Mueller, J.D. (2012) Chromophore maturation and fluorescence fluctuation spectroscopy of fluorescent proteins in a cell-free expression system. *Analytical Biochemistry*, 421, 291–298.
- Mast, Y. & Stegmann, E. (2019) Actinomycetes: the antibiotics producers. *Antibiotics*, 8, 10–13.
- Meyer, V., Basenko, E.Y., Benz, J.P., Braus, G.H., Caddick, M.X., Csukai, M. et al. (2020) Growing a circular economy with fungal biotechnology: a white paper. *Fungal Biology and Biotechnology*, 7, 1–23.
- Minty, J.J., Singer, M.E., Scholz, S.A., Bae, C., Ahn, J., Foster, C.E. et al. (2013) Design and characterization of synthetic fungal-bacterial consortia for direct production of isobutanol from cellulosic biomass. *Proceedings of the National Academy of Sciences*, 110, 1–6.
- Nordholt, N., Van Heerden, J., Kort, R. & Bruggeman, F.J. (2017) Effects of growth rate and promoter activity on single-cell protein expression. *Scientific Reports*, 7, 1–11.
- Ödman, P., Johansen, C.L., Olsson, L., Gernaey, K.V., Lantz, A.E., Lindvald, C. et al. (2009) On-line estimation of biomass, glucose and ethanol in *Saccharomyces cerevisiae* cultivations using in-situ multi-wavelength fluorescence and software sensors. *Journal of Biotechnology*, 144, 102–112.
- Penttilä, M., Nevalainen, H., Rättö, M., Salminen, E. & Knowles, J. (1987) A versatile transformation system for the cellulolytic filamentous fungus *Trichoderma reesei*. *Gene*, 61, 155–164.
- Pöhlker, C., Huffman, J.A. & Pösch, U. (2012) Autofluorescence of atmospheric bioaerosols—Fluorescent biomolecules and potential interferences. *Atmospheric Measurement Techniques*, 5, 37–71.
- Rantasalo, A., Landowski, C.P., Kuivanen, J., Korppoo, A., Reuter, L., Koivistoinen, O. et al. (2018) A universal gene expression system for fungi. *Nucleic Acids Research*, 46, 1–15.
- Roberts, T.M., Rudolf, F., Meyer, A., Pellaux, R., Whitehead, E., Panke, S. et al. (2016) Identification and characterisation of a pH-stable GFP. *Scientific Reports*, 6, 1–9.
- Schlembach, I., Grünberger, A., Rosenbaum, M.A. & Regestein, L. (2021) Measurement techniques to resolve and control population dynamics of mixed-culture processes. *Trends in Biotechnology*, 39, 1093–1109.
- Scholz, S.A., Graves, I., Minty, J.J. & Lin, X.N. (2018) Production of cellulosic organic acids via synthetic fungal consortia. *Biotechnology and Bioengineering*, 115, 1096–1100.
- Shahab, R.L., Luterbacher, J.S., Brethauer, S., Hans, M. & Studer, P. (2018) Consolidated bioprocessing of lignocellulosic biomass to lactic acid by a synthetic fungal-bacterial consortium. *Biotechnology and Bioengineering*, 115, 1207–1215.
- Shaner, N.C., Steinbach, P.A. & Tsien, R.Y. (2005) A guide to choosing fluorescent proteins. *Nature Methods*, 2, 905–909.
- Shinoda, H., Shannon, M. & Nagai, T. (2018) Fluorescent proteins for investigating biological events in acidic environments. *International Journal of Molecular Sciences*, 19, 1548–1567.
- Sun, J., Kelemen, G.H., Fernández-Abalos, J.M. & Bibb, M.J. (1999) Green fluorescent protein as a reporter for spatial and temporal gene expression in *Streptomyces coelicolor* A3(2). *Microbiology*, 145, 2221–2227.
- Surribas, A., Montesinos, J.L. & Valero, F.F. (2006) Biomass estimation using fluorescence measurements in *Pichia pastoris* bioprocess. *Journal of Chemical Technology and Biotechnology*, 81, 23–28.
- Tenconi, E., Guichard, P., Motte, P., Matagne, A. & Rigali, S. (2013) Use of red autofluorescence for monitoring prodigiosin biosynthesis. *Journal of Microbiological Methods*, 93, 138–143.
- Veiter, L. & Herwig, C. (2019) The filamentous fungus penicillium chrysogenum analysed via flow cytometry—a fast and statistically sound insight into morphology and viability. *Applied Microbiology and Biotechnology*, 103, 6725–6735.
- Veiter, L., Kager, J. & Herwig, C. (2020) Optimal process design space to ensure maximum viability and productivity in penicillium chrysogenum pellets during fed-batch cultivations through morphological and physiological control. *Microbial Cell Factories*, 19, 1–14.
- Zacchetti, B., Wösten, H.A.B. & Claessen, D. (2018) Multiscale heterogeneity in filamentous microbes. *Biotechnology Advances*, 36, 2138–2149.
- Zhao, C., Chen, S. & Fang, H. (2018) Consolidated bioprocessing of lignocellulosic biomass to itaconic acid by metabolically engineering *Neurospora crassa*. *Journal of Applied Microbiology*, 102, 9577–9584.

SUPPORTING INFORMATION

Additional supporting information can be found online in the Supporting Information section at the end of this article.

How to cite this article: Palacio-Barrera, A.M., Schlembach, I., Finger, M., Büchs, J. & Rosenbaum, M.A. (2022) Reliable online measurement of population dynamics for filamentous co-cultures. *Microbial Biotechnology*, 15, 2773–2785. Available from: <https://doi.org/10.1111/1751-7915.14129>